



Data Descriptor

UAV-Based 3D Point Clouds of Freshwater Fish Habitats, Xingu River Basin, Brazil

Margaret Kalacska^{1,*}, Oliver Lucanus², Leandro Sousa², Thiago Vieira²  and Juan Pablo Arroyo-Mora³ 

¹ Applied Remote Sensing Lab, Department of Geography, McGill University, Montreal, QC H3A 0B9, Canada

² Laboratório de Ictiologia de Altamira, Universidade Federal do Pará, Altamira PA 68372040, Brazil; oliver.lucanus2@mcgill.ca (O.L.); leandro.m.sousa@gmail.com (L.S.); thiagobernardi007@gmail.com (T.V.)

³ Flight Research Lab, National Research Council Canada, Ottawa, ON K1A 0R6, Canada; juanpablo.arroyo-mora@nrc-cnrc.gc.ca

* Correspondence: margaret.kalacska@mcgill.ca; Tel.: +1-(514)-398-4347

Received: 9 December 2018; Accepted: 7 January 2019; Published: 10 January 2019



Abstract: Dense 3D point clouds were generated from Structure-from-Motion Multiview Stereo (SfM-MVS) photogrammetry for five representative freshwater fish habitats in the Xingu river basin, Brazil. The models were constructed from Unmanned Aerial Vehicle (UAV) photographs collected in 2016 and 2017. The Xingu River is one of the primary tributaries of the Amazon River. It is known for its exceptionally high aquatic biodiversity. The dense 3D point clouds were generated in the dry season when large areas of aquatic substrate are exposed due to the low water level. The point clouds were generated at ground sampling distances of 1.20–2.38 cm. These data are useful for studying the habitat characteristics and complexity of several fish species in a spatially explicit manner, such as calculation of metrics including rugosity and the Minkowski–Bouligand fractal dimension (3D complexity). From these dense 3D point clouds, substrate complexity can be determined more comprehensively than from conventional arbitrary cross sections.

Dataset:

https://figshare.com/articles/3D_Point_Cloud_-_Cachoeira_Xada_Xingu_River_Brazil/7411907

https://figshare.com/articles/Iriri_HD_Ias/7411832

https://figshare.com/articles/3D_Point_Cloud_-_Retroculus_Island_Xingu_River_Brazil/7413314

https://figshare.com/articles/3D_Point_Cloud_Culuene_rapids_Xingu_River_Basin_Brazil/7413371

https://figshare.com/articles/3D_Point_Cloud_-_Jatoba_River_Xingu_River_Basin_Brazil/7413695

Dataset License: CC-BY 4.0.

Keywords: structure from motion; Iriri rapids; Jatoba river; Culuene rapids; Retroculus island; unmanned aerial vehicle; freshwater fish; habitat complexity

1. Summary

The Unmanned Aerial Vehicle (UAV)-based photographs used to create the dense three-dimensional (3D) point clouds described here were collected in August 2016 and August 2017, at five locations in the Xingu river basin: Iriri rapids, Retroculus island, Xada rapids, Jatoba river, and Culuene rapids (Figure 1). As described in [1], these sites represent a range of habitat complexity and classes important for the Xingu's fish diversity. The data described here were used to calculate habitat complexity metrics such as rugosity, the autocorrelation of the surface topographic variation [2,3], and the Minkowski–Bouligand fractal dimension as a measure of 3D complexity [4]. These serve as indicators of the amount of available habitat and shelter for the benthic

organisms, and the amount of brood care and foraging area for mobile species. Raster digital surface models and metrics of texture interpolated from these dense 3D point clouds were further used in a shallow neural network classification to determine the area of specific habitat classes important for the Xingu fish species, such as *sand and pebbles* (grain size <0.5 cm) and *large boulders* (grain size 50–300 cm). The data were further used to compare the conventional estimation of habitat complexity (i.e., chain-and-tape) [5,6] to the spatially explicit 3D reconstructions.

UAV-based photography and 3D reconstruction of terrestrial environments using Structure-from-Motion (SfM) photogrammetry have become increasingly common [7–10]. The concepts have further been applied underwater in marine ecosystems, predominantly to study coral reefs [5,11–13] and deep-sea structures [14]. In a strict sense, our use of the term SfM refers to an analytical workflow that combines both SfM and Multiview Stereo (MVS) photogrammetry, as such, we refer to the methodology as SfM-MVS. In aquatic ecosystems, biodiversity is strongly related to a habitat's structural complexity [15–18]. In freshwater, mapping and distinguishing substrate types is of fundamental importance to the ichthyofauna that either prefer or have obligate associations to certain habitat types (e.g., large boulders vs. sand). Kalacska, M. et al. [1] showed for the first time the applicability of UAV-based SfM-MVS for freshwater fish habitat complexity characterization; the data described herein comprise those models.

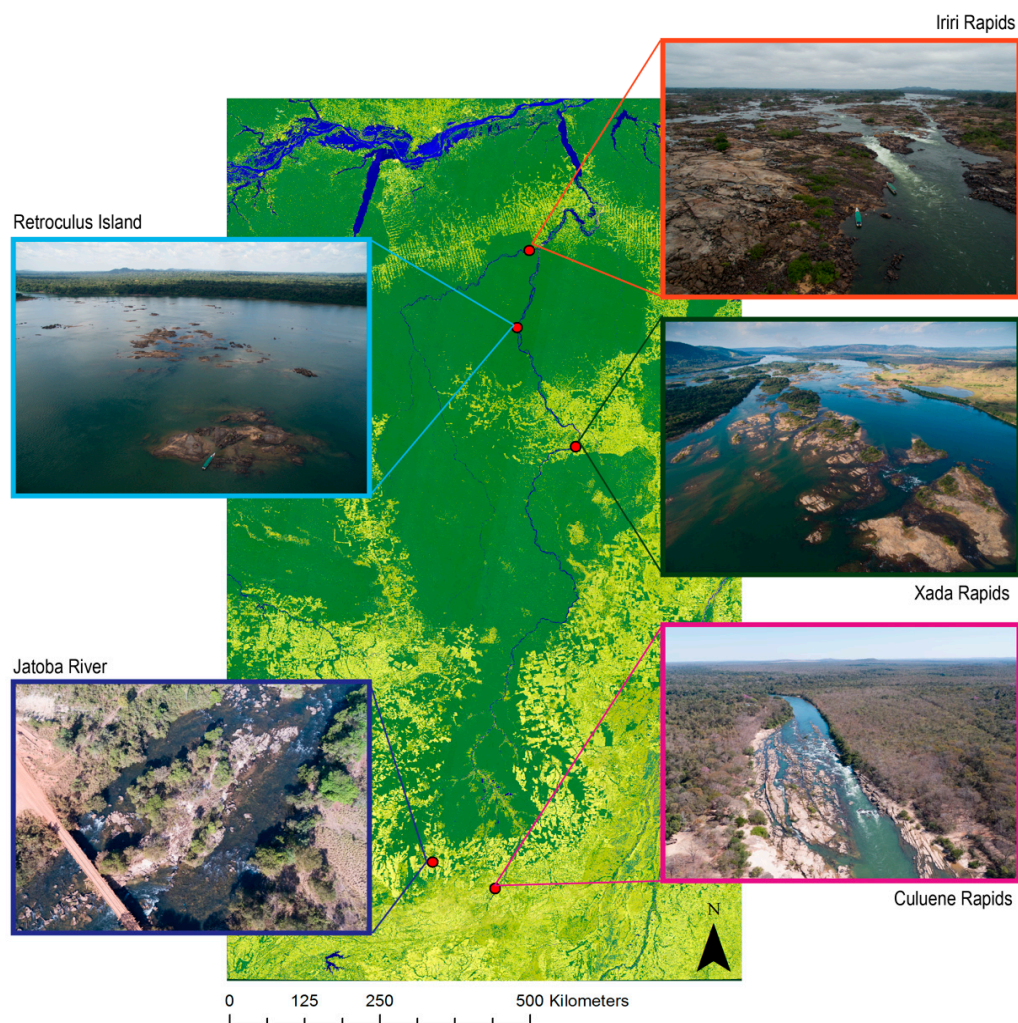


Figure 1. Locations within the Xingu river basin where the five datasets representing a range of freshwater fish habitat complexity and diversity were collected. Background image illustrates the extent of forest cover (green) in the region from 2017, overlaid on a satellite image mosaic from Landsat 8 OLI.

2. Data Description

The data are available for download in .las format [19] with a separate point cloud for each location (Table 1). The data are in a geographic projection (latitude/longitude) with WGS84 as the horizontal datum and EGM96 for the geoid. All height values represent orthometric height in meters. The six columns within the .las file are X,Y,Z positions and R,G,B color values.

Table 1. 3D point cloud files available for download.

File	Location	Size	Interactive version
Jatoba.las	Jatoba river	1.12 GB	http://bit.ly/riojatoba
Culuene_HD.las	Culuene rapids	801.59 MB	http://bit.ly/culuene
Retroculus_island.las	Retroculus island	714.93 MB	http://bit.ly/retroculus
Xada_HD.las	Xada rapids	459.31 MB	http://bit.ly/xadarapids
Iriri_HD.las	Iriri rapids	2.48 GB	http://bit.ly/iriri3D

3. Methods

Two UAVs models were used to collect the photographs used for generating the 3D models: a DJI Inspire 1 and DJI Inspire 2 (Table 2). The Inspire 1 is a 2.9 kg quadcopter with an X3 FC350 camera and integrated 3-axis gimbal ($\pm 0.03^\circ$). The X3 camera has a 1/2.3" CMOS sensor, a fixed 20 mm lens with a 94° diagonal field of view, and a linear rolling shutter producing an image size of 4000×3000 pixels. The Inspire 2 is a 3.4 kg quadcopter, it was used with an X5S camera which has a micro 4/3 sensor, linear rolling shutter, integrated 3 axis $\pm 0.01^\circ$ gimbal, and a DJI MFT 15 mm/1.7 aspherical lens (72° diagonal field of view) producing an image size of 5280×3956 pixels. Flights were conducted in a double grid pattern (orthogonal flight directions). All photographs were written to disk with the geolocation of the center of the frame, and the altitude in the EXIF data. The photographs were collected with Pix4D Capture as the flight planning application, and flight control software in "Fast Picture Trigger" mode with speed category of "Slow+". In this mode, the UAV does not stop at each waypoint to take the photographs. Overlap and side-lap were set to 85%. All photographs were collected in the dry season when the Xingu River and its tributaries are at the lowest water level, exposing large areas of the substrate. In the wet season these areas serve as critical habitat for several fish species.

Table 2. Summary of UAV photographs used for the generation of the 3D models as modified from [1]. Photographs were collected from 30 m AGL altitude.

Location	UAV	Camera	Date	GSD (cm)	No. Photographs	Area (ha)
Jatoba river	Inspire 2	X5S	2 August 2017	1.20	375	2.80
Culuene rapids	Inspire 2	X5S	1 August 2017	1.75	283	4.54
Retroculus island	Inspire 1	X3	8 August 2016	1.43	208	0.52
Xada rapids	Inspire 1	X3	11 August 2016	2.38	420	4.62
Iriri rapids	Inspire 1	X3	6 August 2016	1.46	425	2.77

As described in [1], the SfM-MVS dense 3D point clouds were generated from UAV photographs with Pix4D Mapper Pro [8,20,21], producing ground sampling distances (GSD) ranging from 1.20–2.38 cm (Table 2 and Figure 2). Pix4D Mapper utilizes a modification of the SIFT algorithm [22,23], where local gradients rather than sample intensities are used to create descriptors of each key point [24]. Rolling shutter effects for the two cameras were corrected for in Pix4D Mapper (Table 3). The movement of the camera positions were approximated by a linear interpolation between the camera positions at the start and finish of the image readout [25]. Following the generation of the initial 3D point cloud, multi-view stereo photogrammetry was implemented to increase the density of the point cloud (Tables 4–8).

Table 3. Rolling shutter statistics as determined by Pix4D Mapper. All values represent the median.

Location	Camera Speed (m/s)	Displacement During Readout (m)	Rolling Shutter Readout Time (ms)
Jatoba river	2.1	0.13	60.63
Culuene rapids	3.4	0.27	80.06
Retroculus island	2.0	0.16	80.90
Xada rapids	2.4	0.15	63.58
Irii rapids	2.0	0.14	72.29

Since there were no GNSS active control stations within 100 km of the study sites, and since during data collection there was limited time available at each site, no post processing correction was applied to the geolocations in the EXIF data, nor were any control points collected on site to improve the absolute geo-positional accuracy of the point clouds. The unmodified geolocation was expected to have an absolute positional error up to 3 m. As described in [1] relative positions and distances (i.e., within model) are estimated to have errors within the ground sampling distance for solid structures (e.g., rocks), as measured on the ground by tape measure. For the original application of these data, the within-model accuracy of the features (e.g., size of rocks) was more important than absolute GNSS positional accuracy.

Table 4. Summary of processing details for the SfM-MVS photogrammetry products. The total processing time includes the initial sparse point cloud and generation of the dense point cloud. The average point cloud density refers to the final densified product. The camera optimization properties represent differences between the initial model of focal length/affine transformation parameters of the camera's sensor, and optics and optimized parameters calculated from the data; values are expected to be less than 5%.

Location	Median Matches per Image	Avg Point Cloud Density (/m ³)	Median Keypoints per Image	Camera Optimization (%)	Total Processing Time	Total Number of Points (Dense Point Cloud)
Jatoba river	17,958.3	1044.0	72,446	0.33	8 h:49 min:58 s	35,432,692
Culuene rapids	23,869.7	620.6	70,893	1.96	6 h:16 min:04s	24,695,393
Retroculus Isl.	23,059.0	1782.1	5342	1.36	21 min:44 s	22,033,200
Xada rapids	18,118.6	469.3	41,835	3.42	1 h:57 min:08 s	14,129,408
Irii rapids *	15,684.2	5863.4	42,048	0.12	25 h:58 min:06 s	78,332,198

* the Irii rapids point cloud was processed at the highest image scale in Pix4D Mapper (Scale: 1) which is substantially slower and requires additional hardware resources. All other models were processed at the default of $\frac{1}{2}$ image size for the scale. The workstation used for the processing the data from Jatoba, Culuene, and Irii consisted of an Intel Core i7-3930 K CPU @ 3.2GHz, 48GB DDR3 RAM @ 842 MHz with a 4095 MB NVIDIA GTX 670 GPU. The data from Retroculus island and Xada were processed with the Pix4D Cloud service (Intel Xeon Platinum 8124M CPU @ 3.00GHz with 69 GB RAM).

Table 5. Difference between the initial and computed image positions. These values do not correspond to the positional accuracy of the 3D point cloud. Values reported in meters.

Location	X: $\mu \pm \sigma$	Y: $\mu \pm \sigma$	Z: $\mu \pm \sigma$
Jatoba river	0.00 \pm 0.99	0.00 \pm 0.89	0.01 \pm 0.32
Culuene rapids	0.00 \pm 1.34	0.00 \pm 1.86	0.00 \pm 2.37
Retroculus Island	0.01 \pm 0.52	0.00 \pm 0.50	0.00 \pm 1.01
Xada rapids	0.00 \pm 0.89	0.00 \pm 0.87	0.00 \pm 0.69
Irii rapids	0.00 \pm 0.60	0.00 \pm 0.60	0.00 \pm 1.00

Table 6. Relative camera position and orientation uncertainties. Values represent $\mu \pm \sigma$.

Location	X (m)	Y (m)	Z (m)	Omega (°)	Phi (°)	Kappa (°)
Jatoba river	0.008 ± 0.003	0.007 ± 0.003	0.004 ± 0.001	0.012 ± 0.004	0.010 ± 0.004	0.003 ± 0.001
Culuene rapids	0.012 ± 0.009	0.012 ± 0.008	0.005 ± 0.003	0.012 ± 0.008	0.010 ± 0.007	0.004 ± 0.002
Retroculus Isl.	0.003 ± 0.001	0.003 ± 0.001	0.002 ± 0.001	0.006 ± 0.002	0.006 ± 0.002	0.003 ± 0.001
Xada rapids	0.004 ± 0.002	0.004 ± 0.002	0.003 ± 0.001	0.005 ± 0.002	0.005 ± 0.002	0.002 ± 0.001
Iriri rapids	0.054 ± 0.032	0.053 ± 0.026	0.022 ± 0.010	0.102 ± 0.048	0.097 ± 0.059	0.025 ± 0.008

Table 7. Block Adjustment Details.

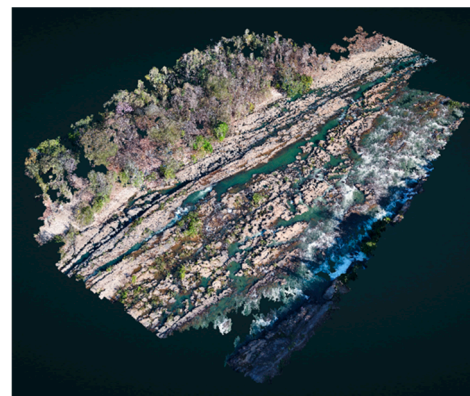
Location	No. 2D Keypoint Observations for Bundle Block Adjustment	No. 3D pts for Bundle Block Adjustment	Mean Reprojection Error (pixels)
Jatoba river	7,021,320	2,165,893	0.205
Culuene rapids	6,436,758	1,293,024	0.198
Retroculus Island	1,353,973	270,069	0.212
Xada rapids	7,668,646	1,442,876	0.259
Iriri rapids	7,720,544	1,848,706	0.199

Table 8. Initial (I) and optimized (O) camera model parameters. Values reported in mm for focal length and x, y principal points. Other parameters are unitless. Uncertainties reported as σ . T = Tangential distortion, R = Radial distortion.

Location	Focal Length	Principal Point x	Principal Point y	R1	R2	R3	T1	T2
Jatoba river	I = 15.000	I = 8.75	I = 6.556	I = 0.000	I = 0.000	I = -0.000	I = 0.000	I = 0.000
	O = 15.065	O = 8.824	O = 6.635	O = -0.005	O = -0.004	O = 0.010	O = 0.001	O = 0.002
	$\sigma = 0.006$	$\sigma = 0.000$	$\sigma = 0.002$	$\sigma = 0.000$	$\sigma = 0.000$	$\sigma = 0.001$	$\sigma = 0.000$	$\sigma = 0.000$
Culuene rapids	I = 15.000	I = 8.75	I = 6.556	I = 0.000	I = 0.000	I = -0.000	I = 0.000	I = 0.000
	O = 14.751	O = 8.854	O = 6.764	O = -0.006	O = -0.004	O = 0.010	O = 0.001	O = 0.002
	$\sigma = 0.004$	$\sigma = 0.000$	$\sigma = 0.002$	$\sigma = 0.000$	$\sigma = 0.000$	$\sigma = 0.000$	$\sigma = 0.000$	$\sigma = 0.000$
Retroculus Island	I = 3.61	I = 3.159	I = 2.369	I = -0.13	I = 0.106	I = -0.016	I = 0.000	I = 0.000
	O = 3.659	O = 3.157	O = 2.356	O = -0.131	O = 0.108	O = -0.014	O = -0.001	O = 0.000
	$\sigma = 0.002$	$\sigma = 0.000$	$\sigma = 0.000$	$\sigma = 0.000$	$\sigma = 0.000$	$\sigma = 0.000$	$\sigma = 0.000$	$\sigma = 0.000$
Xada rapids	I = 3.61	I = 3.159	I = 2.369	I = -0.13	I = 0.106	I = -0.016	I = 0.000	I = 0.000
	O = 3.486	O = 3.156	O = 2.352	O = -0.119	O = 0.087	O = -0.009	O = -0.001	O = 0.000
	$\sigma = 0.001$	$\sigma = 0.000$	$\sigma = 0.000$	$\sigma = 0.000$	$\sigma = 0.000$	$\sigma = 0.000$	$\sigma = 0.000$	$\sigma = 0.000$
Iriri rapids	I = 3.551	I = 3.085	I = 2.314	I = -0.13	I = 0.106	I = -0.016	I = 0.000	I = 0.000
	O = 3.547	O = 3.084	O = 2.300	O = -0.119	O = 0.104	O = -0.013	O = -0.001	O = 0.000
	$\sigma = 0.000$	$\sigma = 0.000$	$\sigma = 0.000$	$\sigma = 0.000$	$\sigma = 0.001$	$\sigma = 0.000$	$\sigma = 0.000$	$\sigma = 0.000$



(A)



(B)

Figure 2. Cont.

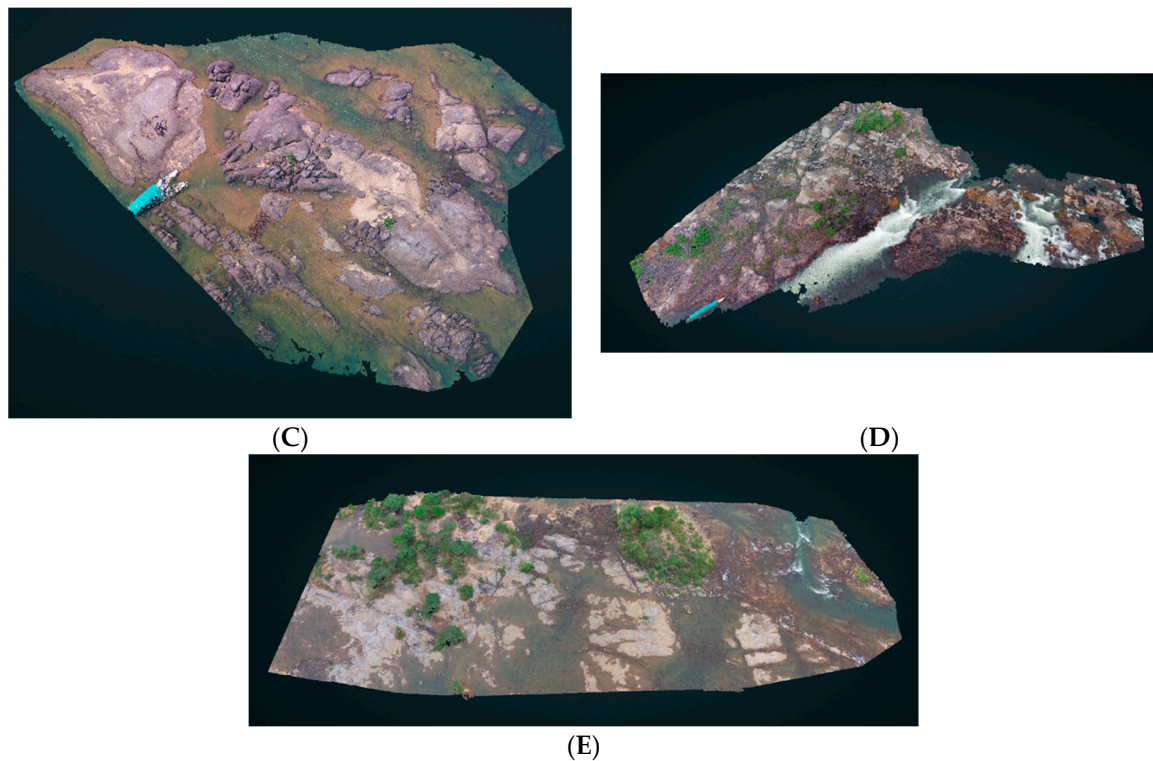


Figure 2. Dense 3D point clouds of the five freshwater habitats in the Xingu river basin. (A) Jatoba river; (B) Culune rapids; (C) Retroculus island; (D) Iriri rapids; and (E) Xada rapids.

4. Limitations

The photographs were collected at nadir, therefore habitat elements such as caves, crevices, the underside of overhangs, areas underneath the vegetation, or tunnels and cracks inside boulders, or other structures underneath or between boulders are either only partially represented or remain data deficient. Areas of fast-moving white water may also show as data deficient, as it was not possible to reconstruct the model in those areas. In the analyses of these data for fish habitat complexity, due to the low water levels, the areas of interest at the sites were comprised of dry exposed substrate everywhere except Jatoba. At Jatoba, because the area of interest had shallow (<1.8 m) water, a refractive index submerged digital surface model correction was applied as per [26–28] prior to the calculation of the habitat complexity metrics.

5. Conclusions

These dense 3D point clouds are digital reconstructions encompassing the most common aquatic habitat classes important for endemic Xingu fishes. The area is spatially explicit and provides a high level of detail from which the habitats can be studied. As shown by [4,5,12,13], in marine environments, and was also found by [1], the complexity metrics calculated from 3D surface reconstructions are more robust than conventional measures. The photographs used to generate these point clouds were collected from low altitude (30 m AGL) UAV flights. Small, light-weight UAVs can be successfully used in remote areas to generate 3D reconstructions of freshwater aquatic habitats.

Author Contributions: Conceptualization, M.K., O.L. and L.S.; methodology, M.K., O.L., and L.S.; formal analysis, M.K.; investigation, M.K., O.L., L.S., T.V. and P.A.; resources, M.K., O.L., L.S. and T.V.; writing—original draft preparation, all authors; writing—review and editing, all authors.

Funding: Natural Sciences and Engineering Research Council of Canada, and Discovery Grant Program to Kalacska and CNPq Universal Project #486376/2013-3 to Sousa.

Acknowledgments: We would like to thank Damilton Rodrigues da Costa (Dani) for fieldwork assistance, and Norma Salcedo and Blake Stoughton from Aquatica for camera housing support. We thank the three anonymous Reviewers for their comments which helped improve our manuscript.

Conflicts of Interest: The authors declare no conflicts of interest. The funders had no role in the design of the study; in the collection, analyses, or interpretation of data; in the writing of the manuscript, or in the decision to publish the results.

References

1. Kalacska, M.; Lucanus, O.; Sousa, L.M.; Vieira, T.; Arroyo-Mora, J.P. Freshwater fish habitat complexity mapping using above and underwater structure-from-motion photogrammetry. *Remote Sens.* **2018**, *10*, 1912. [[CrossRef](#)]
2. Du Preez, C. A new arc-chord ratio (ACR) rugosity index for quantifying three-dimensional landscape structural complexity. *Landsc. Ecol.* **2015**, *30*, 181–192. [[CrossRef](#)]
3. Walbridge, S.; Slocum, N.; Pobuda, M.; Wright, D.J. Unified Geomorphological Analysis Workflows with Benthic Terrain Modeler. *Geosciences* **2018**, *8*, 94. [[CrossRef](#)]
4. Reichert, J.; Backes, A.R.; Schubert, P.; Wilke, T. The power of 3D fractal dimensions for comparative shape and structural complexity analyses of irregularly shaped organisms. *Methods Ecol. Evol.* **2017**, *8*, 1650–1658. [[CrossRef](#)]
5. Leon, J.X.; Roelfsema, C.M.; Saunders, M.I.; Phinn, S.R. Measuring coral reef terrain roughness using ‘Structure-from-Motion’ close-range photogrammetry. *Geomorphology* **2015**, *242*, 21–28. [[CrossRef](#)]
6. McCormick, M.I. Comparison of field methods for measuring surface-topography and their associations with a tropical reef fish assemblage. *Mar. Ecol. Prog. Ser.* **1994**, *112*, 87–96. [[CrossRef](#)]
7. Anderson, K.; Gaston, K.J. Lightweight unmanned aerial vehicles will revolutionize spatial ecology. *Front. Ecol. Environ.* **2013**, *11*, 138–146. [[CrossRef](#)]
8. Cunliffe, A.M.; Brazier, R.E.; Anderson, K. Ultra-fine grain landscape-scale quantification of dryland vegetation structure with drone-acquired structure-from-motion photogrammetry. *Remote Sens. Environ.* **2016**, *183*, 129–143. [[CrossRef](#)]
9. Linchant, J.; Lisein, J.; Semeki, J.; Lejeune, P.; Vermeulen, C. Are unmanned aircraft systems (UASs) the future of wildlife monitoring? A review of accomplishments and challenges. *Mammal Rev.* **2015**, *45*, 239–252. [[CrossRef](#)]
10. Micheletti, N.; Chandler, J.H.; Lane, S.N. Structure from Motion (SfM) Photogrammetry. In *Geomorphological Techniques*; British Society for Geomorphology: London, UK, 2015; pp. 2–12.
11. House, J.E.; Brambilla, V.; Bidaut, L.M.; Christie, A.P.; Pizarro, O.; Madin, J.S.; Dornelas, M. Moving to 3D: Relationships between coral planar area, surface area and volume. *PeerJ* **2018**, *6*, 19. [[CrossRef](#)]
12. Palma, M.; Casado, M.R.; Pantaleo, U.; Cerrano, C. High Resolution Orthomosaics of African Coral Reefs: A Tool for Wide-Scale Benthic Monitoring. *Remote Sens.* **2017**, *9*, 705. [[CrossRef](#)]
13. Young, G.C.; Dey, S.; Rogers, A.D.; Exton, D. Cost and time-effective method for multiscale measures of rugosity, fractal dimension, and vector dispersion from coral reef 3D models. *PLoS ONE* **2017**, *12*, e0175341. [[CrossRef](#)] [[PubMed](#)]
14. Singh, H.; Roman, C.; Pizarro, O.; Eustice, R.; Can, A. Towards high-resolution imaging from underwater vehicles. *Int. J. Robot. Res.* **2007**, *26*, 55–74. [[CrossRef](#)]
15. Ferrari, R.; Bryson, M.; Bridge, T.; Hustache, J.; Williams, S.B.; Byrne, M.; Figueira, W. Quantifying the response of structural complexity and community composition to environmental change in marine communities. *Glob. Chang. Boil.* **2016**, *22*, 1965–1975. [[CrossRef](#)] [[PubMed](#)]
16. Fonseca, V.P.; Pennino, M.G.; de Nobrega, M.F.; Oliveira, J.E.L.; Mendes, L.D. Identifying fish diversity hot-spots in data-poor situations. *Mar. Environ. Res.* **2017**, *129*, 365–373. [[CrossRef](#)]
17. Gonzalez-Rivero, M.; Harborne, A.R.; Herrera-Reveles, A.; Bozec, Y.M.; Rogers, A.; Friedman, A.; Ganase, A.; Hoegh-Guldberg, O. Linking fishes to multiple metrics of coral reef structural complexity using three-dimensional technology. *Sci. Rep.* **2017**, *7*, 13965. [[CrossRef](#)] [[PubMed](#)]
18. Taniguchi, H.; Tokeshi, M. Effects of habitat complexity on benthic assemblages in a variable environment. *Freshw. Boil.* **2004**, *49*, 1164–1178. [[CrossRef](#)]
19. ASPRS. *LAS Specification v 1.2*; ASPRS: Bethesda, MD, USA, 2008.

20. Dandois, J.P.; Olano, M.; Ellis, E.C. Optimal Altitude, Overlap, and Weather Conditions for Computer Vision UAV Estimates of Forest Structure. *Remote Sens.* **2015**, *7*, 13895–13920. [[CrossRef](#)]
21. Kalacska, M.; Chmura, G.L.; Lucanus, O.; Berube, D.; Arroyo-Mora, J.P. Structure from motion will revolutionize analyses of tidal wetland landscapes. *Remote Sens. Environ.* **2017**, *199*, 14–24. [[CrossRef](#)]
22. Lowe, D.G. Distinctive image features from scale-invariant keypoints. *Int. J. Comput. Vis.* **2004**, *60*, 91–110. [[CrossRef](#)]
23. Strecha, C.; von Hansen, W.; Van Gool, L.; Fua, P.; Thoennessen, U. On Benchmarking camera calibration and multi-view stereo for high resolution imagery. In Proceedings of the 2008 IEEE Conference on Computer Vision and Pattern Recognition, Anchorage, AK, USA, 23–28 June 2008.
24. Strecha, C.; Bronstein, A.M.; Bronstein, M.M.; Fua, P. LDAHash: Improved Matching with Smaller Descriptors. *IEEE Trans. Pattern Anal. Mach. Intell.* **2012**, *34*, 66–78. [[CrossRef](#)] [[PubMed](#)]
25. Vautherin, J.; Rutishauser, S.; Schneider-Zapp, K.; Choi, H.F.; Chovancova, V.; Glass, A.; Strecha, C. Photogrammetric accuracy and modeling of rolling shutter cameras. *ISPRS J. Photogramm. Remote Sens.* **2016**, *3*, 139–146. [[CrossRef](#)]
26. Tamminga, A.; Hugenholtz, C.; Eaton, B.; Lapointe, M. Hyperspatial remote sensing of channel reach morphology and hydraulic fish habitat using an unmanned aerial vehicle (UAV): A first assessment in the context of river research and management. *River Res. Appl.* **2015**, *31*, 379–391. [[CrossRef](#)]
27. Westaway, R.M.; Lane, S.N.; Hicks, D.M. The development of an automated correction procedure for digital photogrammetry for the study of wide, shallow, gravel-bed rivers. *Earth Surf. Process. Landf.* **2000**, *25*, 209–226. [[CrossRef](#)]
28. Woodget, A.S.; Carbonneau, P.E.; Visser, F.; Maddock, I.P. Quantifying submerged fluvial topography using hyperspatial resolution UAS imagery and structure from motion photogrammetry. *Earth Surf. Process. Landf.* **2015**, *40*, 47–64. [[CrossRef](#)]



© 2019 by the authors. Licensee MDPI, Basel, Switzerland. This article is an open access article distributed under the terms and conditions of the Creative Commons Attribution (CC BY) license (<http://creativecommons.org/licenses/by/4.0/>).